



## Revised atmospheric excitation function series related to Earth's variable rotation under consideration of surface topography

Y. H. Zhou,<sup>1,2</sup> D. A. Salstein,<sup>3,4</sup> and J. L. Chen<sup>5</sup>

Received 23 August 2005; revised 22 February 2006; accepted 22 March 2006; published 29 June 2006.

[1] The atmospheric angular momentum is closely related to variations in the Earth rotation. The atmospheric excitation function (AEF), known also as the atmospheric effective angular momentum function, is introduced in studying the atmospheric excitation of the Earth's variable rotation. It may be separated into two portions, i.e., the “wind” terms due to the atmospheric motion relative to the mantle and the “pressure” terms due to the variations of atmospheric mass distribution evident through surface pressure changes. The AEF wind terms during the period of 1948–2004 are reprocessed from the National Centers for Environmental Prediction-National Center for Atmospheric Research (NCEP/NCAR) reanalysis 6-hourly wind and pressure fields. Some previous calculations were approximate, in that the wind terms were integrated from an isobaric lower boundary of 1000 hPa. To consider the surface topography effect, however, the AEF is computed by integration using the winds from the Earth's surface to 10 hPa, the top atmospheric model level, instead of from 1000 hPa. For these two cases, only a minor difference, equivalent to  $\sim 0.004$  ms in length-of-day variation, exists with respect to the axial wind term. However, considerable differences, equivalent to 5–6 milliseconds of arc in polar motion, are found regarding equatorial wind terms. We further compare the total equatorial AEF (with and without the topography effect) with the polar motion excitation function (PMEF) during the period of 1980–2003. The equatorial AEF gets generally closer to the PMEF, and improved coherences are found between them when the topography effect is included.

**Citation:** Zhou, Y. H., D. A. Salstein, and J. L. Chen (2006), Revised atmospheric excitation function series related to Earth's variable rotation under consideration of surface topography, *J. Geophys. Res.*, *111*, D12108, doi:10.1029/2005JD006608.

### 1. Introduction

[2] The dynamic interactions that occur between atmosphere and solid Earth are related globally by conservation of angular momentum in the Earth system. Owing to this condition, the global atmospheric angular momentum variation is closely related to the Earth's variable rotation on timescales between a few days and several years [e.g., Barnes *et al.*, 1983; Eubanks *et al.*, 1988; Chao and Au, 1991; Hide and Dickey, 1991; Zhou *et al.*, 2001]. The atmospheric excitation function (AEF), namely the atmospheric effective angular momentum function in the work of Barnes *et al.* [1983], is introduced in studying the atmospheric excitation of the Earth's variable rotation. Obtaining

accurate calculations of AEF is thus of great interest to the geodetic community, which is concerned with Earth's rotation and its reference frame. The AEF has three components: an axial component, related to the rate of rotation of Earth and measured by length of day (LOD), and two equatorial components, related to the motion of the pole in an Earth-fixed reference frame. Each component has “wind” and “pressure” terms reflecting atmospheric relative angular momentum and the redistribution of global atmospheric mass. The AEF is usually calculated from global atmospheric analysis or reanalysis fields from a four-dimensional data assimilation system that incorporates a heterogeneous set of data and an underlying atmospheric model. These series based on four of the world's major meteorological centers have been archived by the Special Bureau for Atmosphere (SBA) of the Global Geophysical Fluids Center of the International Earth Rotation and Reference Systems Service (IERS) [Salstein *et al.*, 1993; Salstein and Rosen, 1997].

[3] Substantial discrepancies exist among the AEF collected from output of the analyses by several of the world meteorological centers. Hide *et al.* [1997] stated that the dominant seasonal error in simulating the axial AEF is an underestimation of AEF during northern hemisphere winter associated with errors in the position of subtropical jets. Eubanks *et al.* [1988] found that the two equatorial AEF

<sup>1</sup>Shanghai Astronomical Observatory, Chinese Academy of Sciences, Shanghai, China.

<sup>2</sup>Also at Atmospheric and Environmental Research, Inc., Lexington, Massachusetts, USA.

<sup>3</sup>Atmospheric and Environmental Research, Inc., Lexington, Massachusetts, USA.

<sup>4</sup>NASA Goddard Space Flight Center, University of Maryland Baltimore Campus, Greenbelt, Maryland, USA.

<sup>5</sup>Center for Space Research, University of Texas at Austin, Austin, Texas, USA.

pressure terms from the US National Meteorological Center (NMC) and Japan Meteorological Agency (JMA) have much higher correlation ( $\sim 0.9$ ) than the wind terms ( $\sim 0.4$ ). The large disagreements in these equatorial wind terms were attributed in part to a lack of data from sparsely observed regions such as the South Pacific. In the study of atmospheric contributions to the Earth rotation on the seasonal time scale, *Aoyama and Naito* [2000] demonstrated that the differences in equatorial AEF wind terms between the JMA and the U.S. National Center for Environmental Prediction (NCEP, formerly NMC)/National Center for Atmospheric Research (NCAR) result not only from the discrepancies arising from the different tropospheric regional winds associated with the Asian monsoon but also from the difference in the vertical integration methods of computing AEF wind terms [*Rosen and Salstein*, 1985; *Naito et al.*, 1987, 2000].

[4] Here we reprocess the AEF during the period of 1948–2004 based on the NCEP/NCAR reanalysis wind and pressure fields [*Kalnay et al.*, 1996]. Some previous calculations for the SBA are approximated, with the winds integrated from an isobaric lower boundary at 1000 hPa. To consider the surface topography effect, however, the AEF is computed here by integration using the winds from the Earth's surface to 10 hPa, the top atmospheric model level, instead of from 1000 hPa. This method has been applied in the computation of JMA AEF by using the surface pressures on land and sea level pressures on oceans [*Naito et al.*, 1987]. In section 2, we introduce the basic formulas and data processing of the AEF and the Earth rotation excitation function. The comparisons among the AEF with and without consideration of Earth's topography and the Earth rotation excitations are given in section 3. We summarize the results in section 4.

## 2. Formulation and Data Processing

### 2.1. Earth Rotation Excitation Function

[5] In the terrestrial coordinate system, the rotation of the Earth can be described by the three-dimensional instantaneous angular velocity vector of the mantle. Its axial and equatorial components are associated with the variations of the Earth's rotational rate (or the LOD change) and the polar motion, respectively. The Earth's rotation is basically subject to the following excitation equations, under the conservation of the Earth's total angular momentum [*Barnes et al.*, 1983; *Eubanks*, 1993; *Aoyama and Naito*, 2000]:

$$\mathbf{m} + (i/\sigma_c)\dot{\mathbf{m}} = \boldsymbol{\psi} \quad (1)$$

$$\dot{m}_3 + \dot{\psi}_3 = 0. \quad (2)$$

In equation (1),  $\mathbf{m} = m_1 - im_2$  is a dimensionless complex-valued small quantity representing the Earth's polar motion, where subscripts 1 and 2 refer to the x (along the Greenwich Meridian) and y (along the 90°E longitude) coordinates of the terrestrial frame (the negative sign comes from the left-handed coordinate system in the conventional definition of polar motions  $m_1$  and  $m_2$ ).  $\boldsymbol{\psi} = \psi_1 + i\psi_2$  with  $\psi_1$  and  $\psi_2$  being the x and y components, respectively, of the polar motion excitation function (PMEF),  $\sigma_c = 2\pi F_c(1 + i/2Q)$  is

the complex Chandler frequency,  $F_c$  is about 0.843 cycles per year, and  $Q$  is the damping factor of the Chandler oscillation. In equation (2),  $m_3 = -\Delta\Lambda/\Lambda_0$  is a small dimensionless quantity representing the LOD change, where  $\Lambda_0$  and  $\Delta\Lambda$  are a standard LOD and its deviation, the subscript 3 refers to the z (along the north pole) coordinate of the terrestrial frame, and  $\psi_3$  is the excitation function for the LOD change.

[6] The observed polar motion time series is from the SPACE2003 [*Gross*, 2004] EOP time series, produced by the Jet Propulsion Laboratory, which is daily, sampled at midnight, and covers the period 1976–2003. It is produced through a Kalman filter combination of the Earth orientation measurements from advanced space-geodetic techniques including lunar and satellite laser ranging, very long baseline interferometry, and the global positioning system. The PMEF is computed using equation (1) [*Wilson*, 1985], at a discrete set of time periods, with  $Q = 179$  [*Wilson and Vicente*, 1990].

### 2.2. Atmospheric Excitation Function

[7] Similar to the Earth rotation vector, the AEF has equatorial and axial components ( $\chi$  and  $\chi_3$ ). Each component consists of the pressure term ( $\chi^P, \chi_3^P$ ) due to air mass redistribution, and the wind term ( $\chi^W, \chi_3^W$ ) due to atmospheric relative angular momentum. They are expressed as follows [*Eubanks*, 1993]:

$$\begin{aligned} \chi^P &= \chi_1^P + i\chi_2^P \\ &= \frac{-1.098R^4}{(C-A)g} \iint p_s \sin\phi \cos^2\phi e^{i\lambda} d\lambda d\phi \end{aligned} \quad (3)$$

$$\begin{aligned} \chi^W &= \chi_1^W + i\chi_2^W \\ &= \frac{-1.5913R^3}{\Omega(C-A)g} \iiint (u \sin\phi + iv) \cos\phi e^{i\lambda} dp d\lambda d\phi \end{aligned} \quad (4)$$

$$\chi_3^P = \frac{0.753R^4}{C_m g} \iint p_s \cos^3\phi d\lambda d\phi \quad (5)$$

$$\chi_3^W = \frac{0.998R^3}{C_m \Omega g} \iiint u \cos^2\phi dp d\lambda d\phi, \quad (6)$$

where  $R$  and  $\Omega$  are the Earth's mean radius and angular velocity,  $A$  and  $C$  are the Earth's principal moments of inertia,  $C_m$  is the mantle's principal moment of inertia,  $g$  is gravitational acceleration,  $\lambda$  and  $\phi$  are longitude and latitude at a given grid point,  $p_s$  is surface pressure,  $u$  and  $v$  are the zonal and meridional wind velocities, respectively.

[8] The AEF is computed based on equations (3)–(6), using four-times daily (0000, 0600, 1200, and 1800 GMT) wind and pressure fields for the year of 1948 to 2004, from the NCEP/NCAR reanalysis atmospheric system [*Kalnay et al.*, 1996]. The output is on grid with resolution 2.5° longitude by 2.5° latitude. The wind fields covers 17 pressure levels (1000, 925, 850, 700, 600, 500, 400, 300, 250, 200, 150, 100, 70, 50, 30, 20, and 10 hPa). In

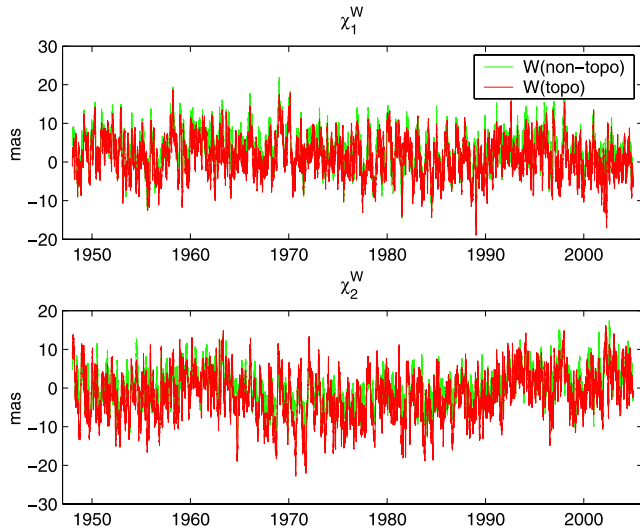


**Figure 1.** The equatorial wind terms ( $\chi_1$  and  $\chi_2$ ) of the atmospheric excitation function (AEF) with/without the surface topography correction (red/green curves) during the period of 1948–2004. For clarity of display, 30-day moving averages of the 6-hourly data are shown. W(nontopo): AEF wind term without consideration of surface topography; W(topo): AEF wind term with consideration of surface topography.

calculating wind terms, we compensate the Earth's topography effect by integrating wind from the NCEP model's variable Earth surface pressure level (not 1000 hPa) to the top (10 hPa) of the model [Naito *et al.*, 1987; Aoyama and Naito, 2000]. Therefore for the integration of winds of bottom layers which are affected by the surface topography, the thickness of air over each grid point on the global Earth would be a spatial variable rather than a constant everywhere. In calculating pressure terms, two extreme cases are considered. One is based on the inverted barometer (IB) assumption, which assumes that oceans respond to the atmospheric loading isostatically; the other is a noninverted barometer (non-IB) assumption, which assumes that oceans behave like a solid surface [Munk and MacDonald, 1960; Salstein *et al.*, 1993]. In order to match the temporal resolution of the PMEF, the 6-hourly NCEP/NCAR reanalysis AEF is averaged daily by summing five consecutive values using weights of 1/8, 1/4, 1/4, 1/4, 1/8.

### 3. Results and Comparison

#### 3.1. Comparison Between AEF Wind Terms During 1948–2004 With and Without Consideration of Surface Topography

[9] The surface topography effect is demonstrated by the comparison between the AEF wind terms with and without the surface topography correction. Figure 1 shows the comparison of equatorial wind terms not accounting for (green curves) and accounting for (red curves) topography (topo) during the period of 1948–2004. The differences of the equatorial wind terms between the nontopo and the topo terms are given in Figure 2. For clarity of display, 30-day moving averages of the 6-hourly data are shown. The standard deviations of the differences are 5.8 and 5.4 milli-seconds of arc (mas) for  $\chi_1$  and  $\chi_2$ , respectively. Figure 3

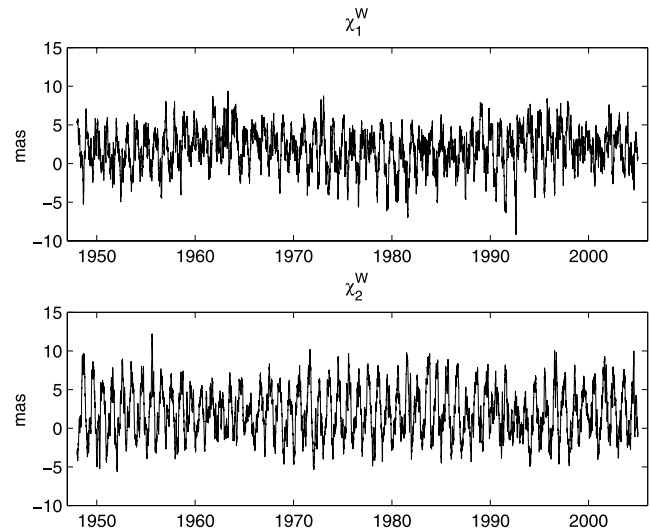


**Figure 2.** Differences between the nontopo and topo equatorial wind terms ( $\chi_1$  and  $\chi_2$ ) shown in Figure 1.

displays the comparison of axial wind terms between the nontopo (green curve) and topo (red curve) cases and the difference between these two terms. The standard deviation of the difference is 0.004 ms. Obviously, only a minor difference between the nontopo and topo cases exists with respect to the axial wind term. However, considerable differences are found regarding the equatorial wind terms. This different characteristic of wind contributions in the axial and equatorial components was also found by Aoyama and Naito [2000] in their study of wind contribution to the Earth's angular momentum budgets on the seasonal time-scale. The equatorial wind AEFs are affected by the zonal and meridional wind field in the lower troposphere, while the axial wind AEF is driven mainly by the prevailing zonal wind circulation in the upper troposphere and stratosphere [Peixoto and Oort, 1992]. In this case, the axial component is influenced relatively little by the wind field inside the

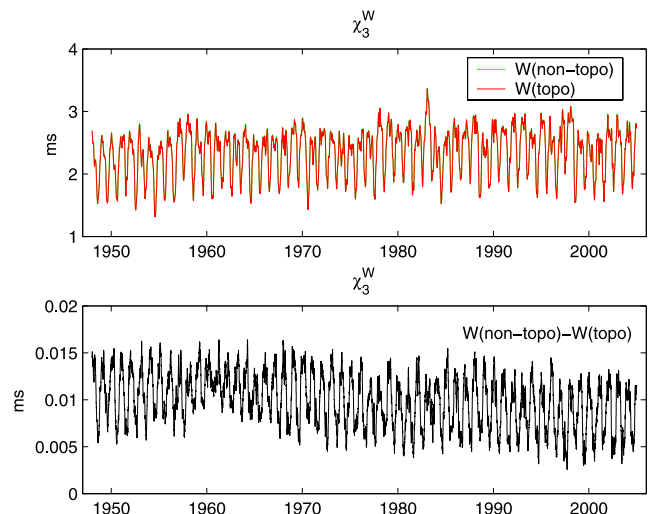


**Figure 3.** The nontopo (green curve) and topo (red curve) axial wind term ( $\chi_3$ ) during the period of 1948–2004 (top) and the difference between these two terms (bottom).

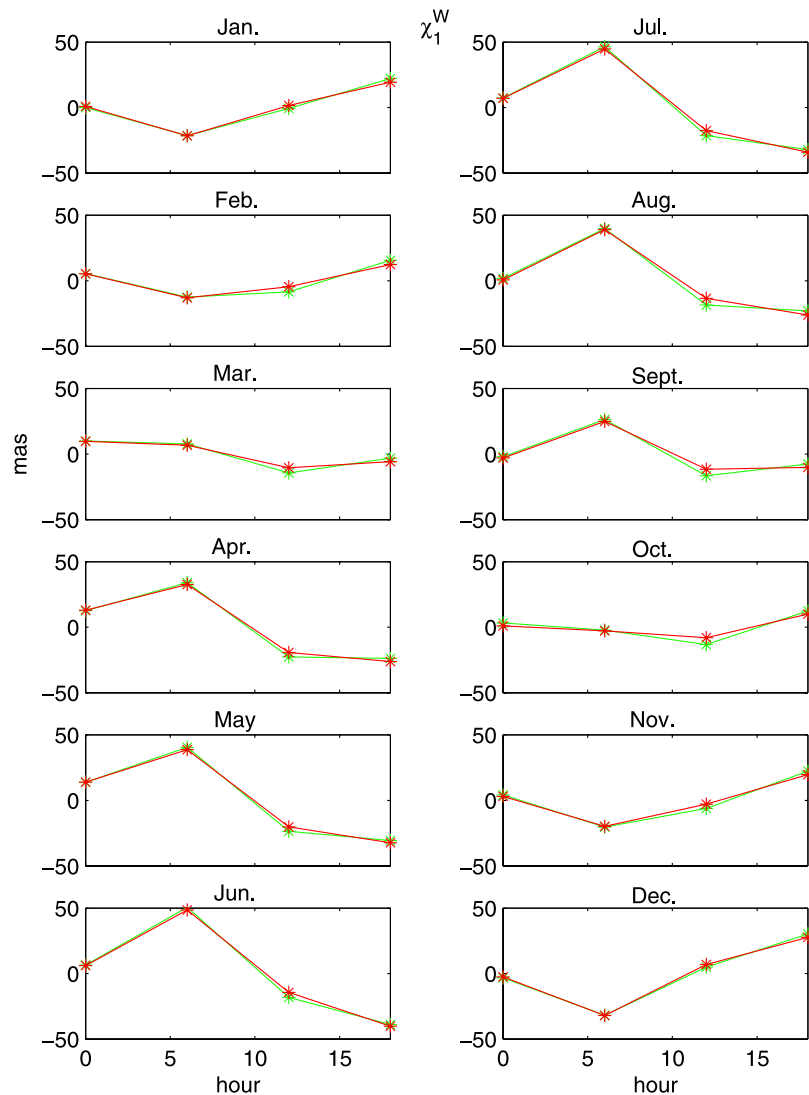


**Figure 4.** Mean daily variation pattern of the equatorial wind term ( $\chi_1^W$ ) with/without the surface topography correction (red/green curves and stars) during all 12 months in 2002.

surface topography. It should be mentioned that the equatorial pressure term, a strong contributor to polar motion excitation, is unaffected by the lower boundary approximation (see equation (3)).

[10] Figures 4 and 5 show mean daily variation patterns (based on 4 synoptic hours: 0, 6, 12, 18) of the equatorial wind terms ( $\chi_1^W$  and  $\chi_2^W$ ) with/without the surface topography correction (red/green curves and stars) during all 12 months in 2002. Atmospheric tides are known to cause daily variations in wind [Hsu and Hoskins, 1989], which transfer here to variations in polar motion excitation. As can be seen, the daily variation pattern is slightly affected by the surface topography. The noticeable surface topography effect (albeit quite small) at 1200 UT on the  $\chi_1$  wind term is consistent with the finding by Hsu and Hoskins [1989] that the diurnal and semidiurnal wind signals in the lower troposphere are affected by thermal effects related to local topography and land-sea contrasts. The equatorial wind terms have strong variations with magnitude of 10~20 mas. They are seasonally modulated and appear to have a distinct “winter mode” (January to February, November to Decem-

ber) and “summer mode” (April to September). The months of March and October appear to be periods of transition between the summer and winter modes. Also shown in Figure 6 is the mean daily variation pattern of the axial wind term ( $\chi_3^W$ ). It has a very small daily variation with magnitude of  $\sim 0.01$  ms. The surface topography effect on this term is negligible throughout the whole period.

[11] It is interesting to see how the surface topography affects the AEF wind terms. As an example, Figure 7 displays a “snapshot” of thickness of air (in unit of hPa) of layers 1~7 (1: surface-962.5 hPa; 2: 962.5–887.5 hPa; 3: 887.5–775 hPa; 4: 775–650 hPa; 5: 650–550 hPa; 6: 550–450 hPa; 7: 450–350 hPa) at 0 hour, 1 January 2003. The amount of topography in each layer is evident. The thickness of air of layer 1 (surface layer) reflects clearly the Earth’s variable topography. From layer 1 to layer 7, we witness the gradual disappearing of the topography. The influence of the Himalayas Mountains is most significant. It goes as high as into layer 6 and disappears at layer 7.

[12] The surface topography effects on the equatorial wind AEFs are demonstrated in Figures 8 and 9. Figure 8

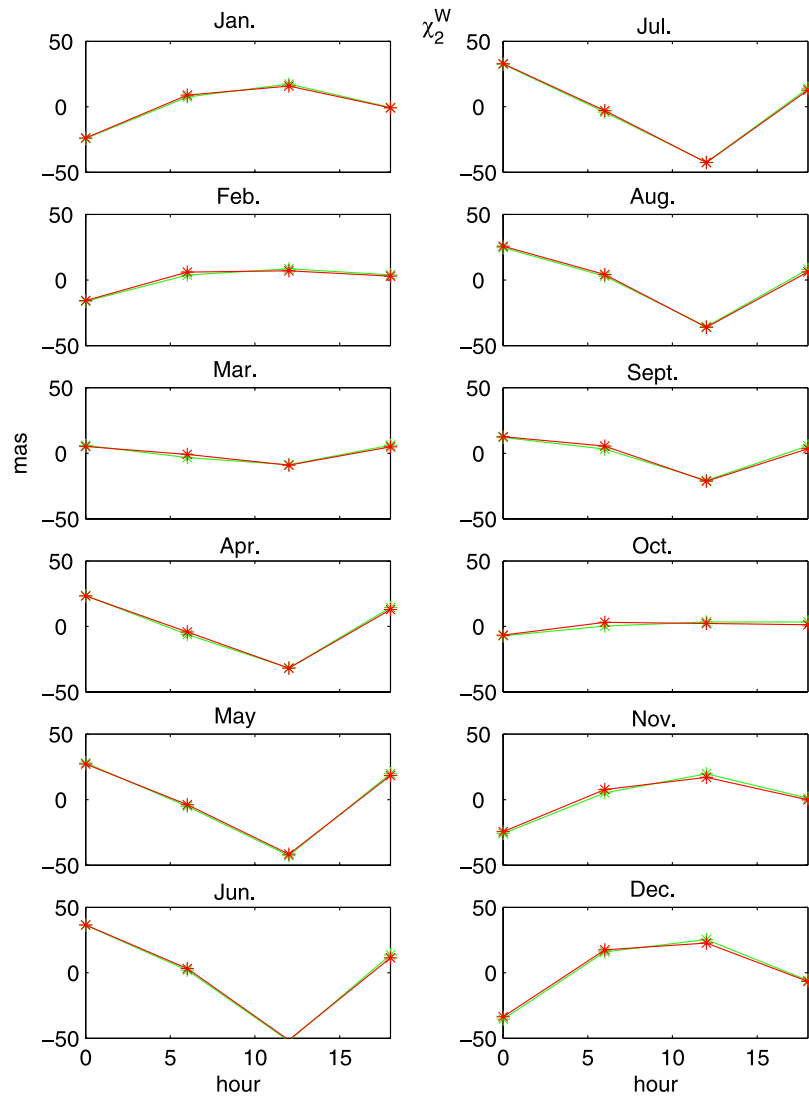


**Figure 5.** As in Figure 4 but for the  $\chi_2^W$  term.

shows the differences between the nontopo and topo  $\chi_1^W$  terms integrated in layers 1~7. The mean value has been removed from each series. For clarity of display, 30-day moving averages of the 6-hourly data are shown. As expected, the difference between the nontopo and topo wind terms finally decreases to zero in layer 7. Also shown in Figure 9 are the differences between the nontopo and topo  $\chi_2^W$  terms. While the strongest annual difference in  $\chi_1^W$  term appears to be in layer 1 (the surface layer), the strongest annual difference in  $\chi_2^W$  term appears in layers 2, 3, and 4. The different impact of the surface topography effect for the two equatorial components results from the non-uniform geographical distribution of the global surface topography and the different spatial patterns of weighting functions given in equation (4).

### 3.2. Comparison Among the AEFs During 1980–2003 With and Without Consideration of Surface Topography and the PMEF

[13] The effect of the Earth's topography on the AEF is revealed by the comparison among the equatorial AEFs during 1980–2003 with and without consideration of sur-

face topography and the PMEF. The comparison for the axial component is omitted as it is affected by topography only in a negligible way. The period of comparison is selected starting from 1980 in consideration that the polar motion observations are greatly enhanced due to applications of modern space geodetic techniques [Gross, 2004]. The meteorological analyses have been enhanced as well by the introduction of space-based observations around that date.

#### 3.2.1. Power and Coherence Spectrum Analysis

[14] The surface topography effect on the equatorial wind AEFs is revealed by the power and coherence spectrum analyses in the frequency domain. Figure 10 shows the power spectra of the equatorial AEF wind terms,  $W(\text{nontopo})$  and  $W(\text{topo})$ , computed by the multitaper method. A linear term has been removed from each series prior to the spectral analysis in the frequency domain. The multitaper technique was first introduced by Thomson [1982], i.e., several windows are added to the time series prior to the Fourier transformation. Although it degrades the spectral resolution, it greatly reduces the spectral leakage and hence provides more reliable spectral estimates [Chao *et al.*,

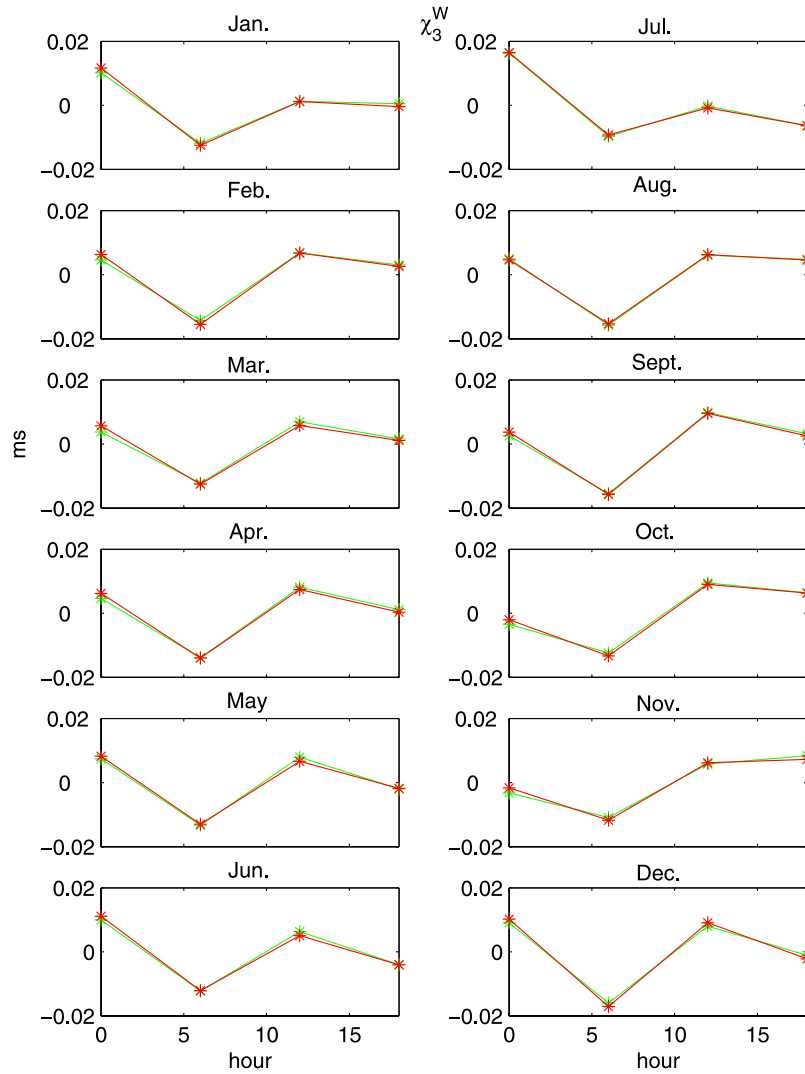


**Figure 6.** As in Figure 4 but for the  $\chi_3^W$  term.

1995]. It can be seen from Figure 10 that the  $W(\text{topo})$  term has generally more power than the  $W(\text{nontopo})$  term except at the annual period (1 cycle/year) for the x-component. Figure 11 shows the power spectra of differences between the  $W(\text{topo})$  and  $W(\text{nontopo})$  terms. Obviously, there are considerable differences over a broad frequency band, in which the largest differences exist in the annual frequency. Although Figure 10 shows that the annual x-component appears to have a larger difference in amplitude between the topo and nontopo terms than does the y-component, owing to the greater annual phase difference for the y-component than for the x-component, the difference plots in Figure 11 shows that the y-component has the larger annual difference between the topo and nontopo terms than does the x-component.

[15] Further comparisons between the AEF (with and without consideration of surface topography) and the PMEF are displayed in Figure 12. The total of AEF wind term and IB pressure term are compared with polar motion excitations. Apparently, considerable discrepancies remain between the AEF and PMEF, which indicate nonatmospheric sources to the polar motion excitation exist, like global

oceans and continental water storage change [Chao and Zhou, 1999; Johnson *et al.*, 1999; Ponte and Stammer, 1999; Gross *et al.*, 2003; Chen *et al.*, 2004; Chen and Wilson, 2005; Zhou *et al.*, 2005]. Moreover, it is interesting to note that adding topography effect brings the AEF generally closer to the PMEF, though only slightly at most frequencies.

[16] To reveal further the topography effect on the annual component of polar motion excitation, shown in Figure 12, we extract the annual component by fitting a linear combination of a trend, annual, semiannual and terannual terms to the AEFs and PMEF in a least squares sense. Table 1 lists the results of this fit for the amplitude  $A$  and phase  $\alpha$  of the prograde (subscript  $p$ ) and retrograde (subscript  $r$ ) components of the excitation of annual polar motion defined by [Munk and MacDonald, 1960]

$$\chi(\mathbf{t}) = A_p e^{i\alpha_p} e^{i\sigma(t-t_0)} + A_r e^{i\alpha_r} e^{-i\sigma(t-t_0)}, \quad (7)$$

where  $\sigma$  is the annual frequency and the reference date  $t_0$  is 1 January 1980, 0000 UT. As is consistent with previous studies [e.g., Gross *et al.*, 2003], for both the prograde and

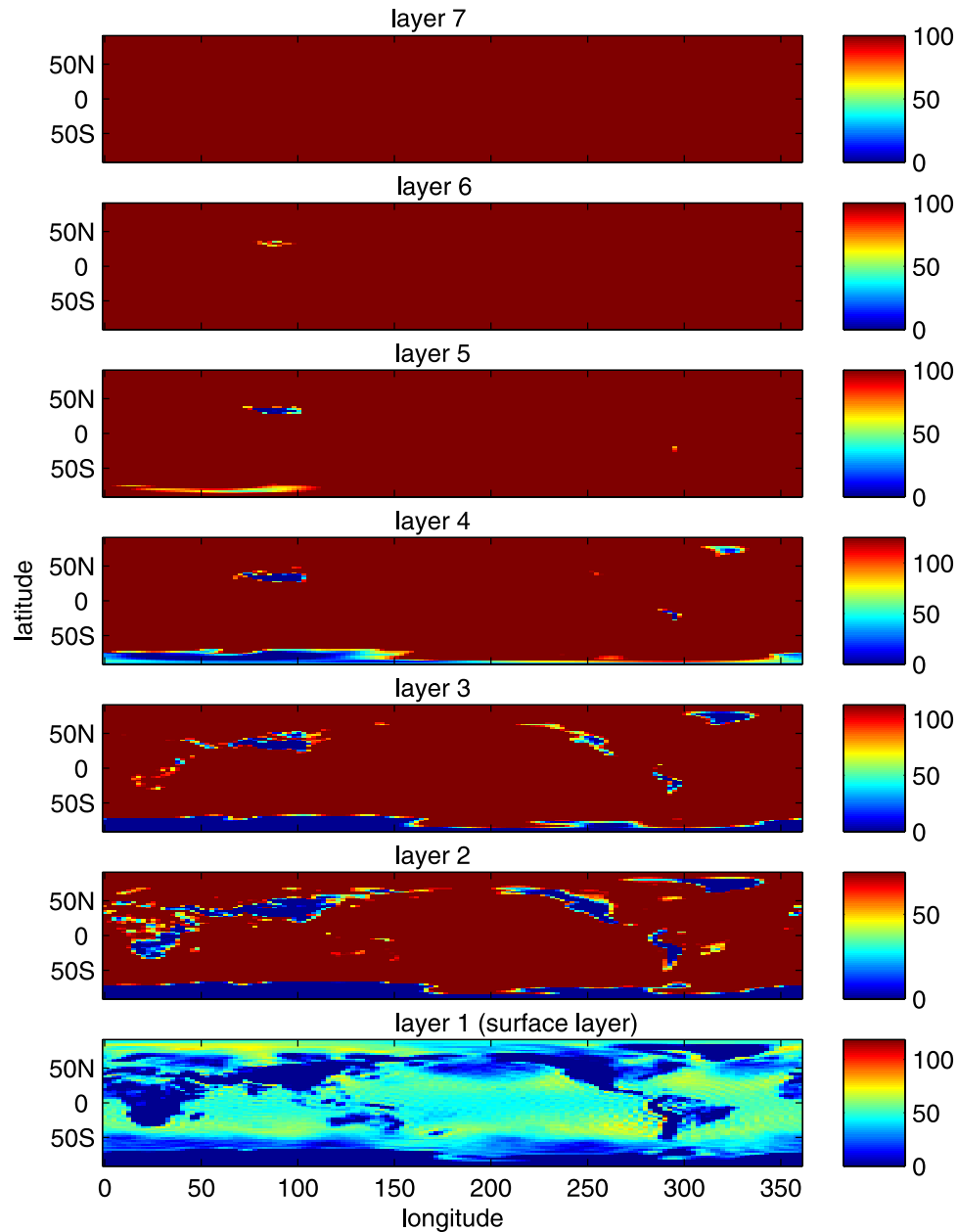


**Figure 7.** The surface topography shown by the thickness of air (in unit of hPa) in layers 1~7 (1: surface-962.5 hPa; 2: 962.5–887.5 hPa; 3: 887.5–775 hPa; 4: 775–650 hPa; 5: 650–550 hPa; 6: 550–450 hPa; 7: 450–350 hPa).

retrograde components, the surface pressure variation is seen to be the dominant excitation mechanism, being more than 5 times as large as the effect of wind based on the NCEP/NCAR reanalysis. The European Centre for Medium-Range Weather Forecasts (ECMWF) and JMA wind AEF shows larger contribution to the annual wobble [e.g. *Masaki and Aoyama, 2005*]. The inclusion of surface topography leads to amplitude reductions of  $\sim 30\%$  and phase changes of  $41^\circ$  and  $106^\circ$  for the prograde and retrograde wind terms, respectively. The total of AEF pressure and wind terms with consideration of surface topography effect appears to be closer to the annual PMEF than that without consideration of surface topography. Figure 13 shows the phasor diagram of the prograde (top)

and retrograde (bottom) annual components of the AEF and PMEF. Apparently, adding topography effect brings the AEF closer to the PMEF on the annual timescale, which is particularly different for the retrograde component.

[17] Figure 14 exhibits the multitaper squared coherences between the AEF (with and without consideration of surface topography) and the PMEF in the frequency domain. A trend and a seasonal signal are removed from each series prior to the coherence analysis. The horizontal dashed line represents the 95% significance level. The vertical dashed line indicates the Chandler frequency of 0.843 cycles per year. When the topography effect is considered, generally improved coherences between the total equatorial AEF and the PMEF are found over a broad frequency band with

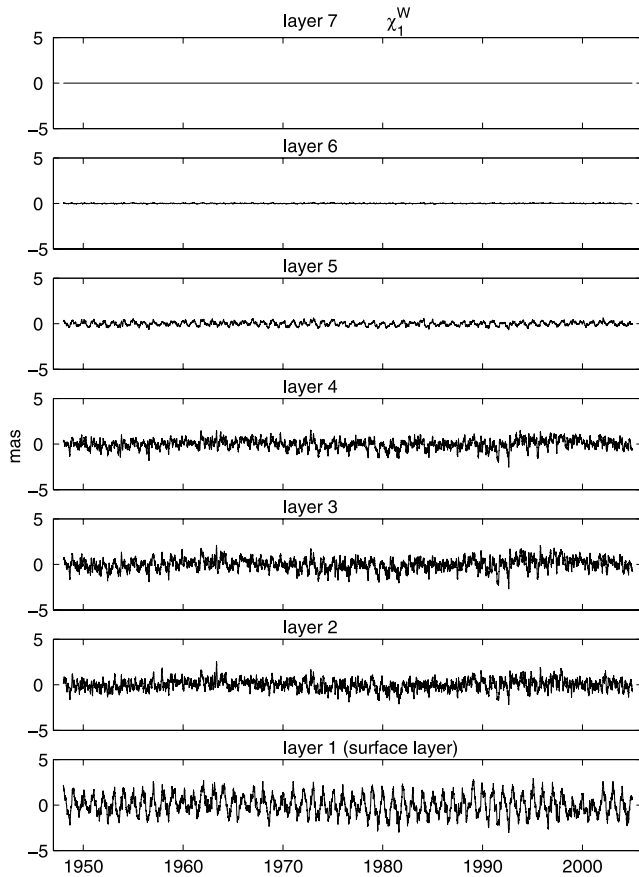


**Figure 8.** Surface topography effects on the equatorial wind AEFs shown by differences between the nontopo and topo  $\chi_1^W$  terms from layers 1 to 7. The mean value has been removed from each series. For purposes of clarity of display, 30-day moving averages of the 6-hourly data are shown.

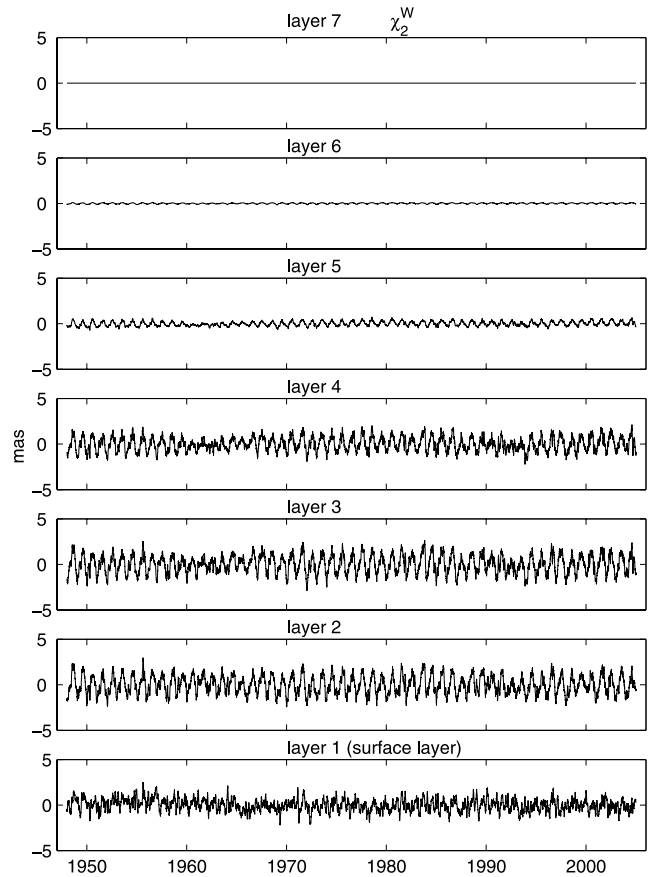


**Figure 9.** As in Figure 8 but for the  $\chi_2^W$  term.

respect to the x-component, though marginal improvements are seen with respect to the y-component. The improved coherences around the Chandler frequency are also evident, which confirms the previous finding of *Aoyama* [2005]. Further analysis on the time domain is given in the following section.

**3.2.2. Correlation and Variance Analysis**

[18] The surface topography effect on the equatorial wind AEFs is revealed by the correlation and variance analyses in the time domain. We first remove from the AEF and PMEF a linear combination of a trend, annual, semiannual, and terannual terms that was fitted by the least squares method. Then, the residual series is passed through a Butterworth high-pass filter of order 2, in both forward and reverse directions to eliminate any phase distortion [Wiley, 1979]. The cutoff frequency is 1 cycle per year. Thus the resulting series is considered as the intraseasonal variation used in the following cross correlation and variance analyses.

[19] Table 2 assembles the cross correlation coefficients between the intraseasonal PMEF and AEF, and variance reductions (in percentage) when the atmospheric effects are removed from the PMEF. X and Y give results for the x and y components, and  $X + iY$  for the complex-values  $x + iy$  component. The surface pressure variation and winds are

both important excitation mechanisms to the intraseasonal polar motion. The surface pressure variation can explain 35.4% of the polar motion excitation and the correlation between them reaches 0.6. After the surface topography

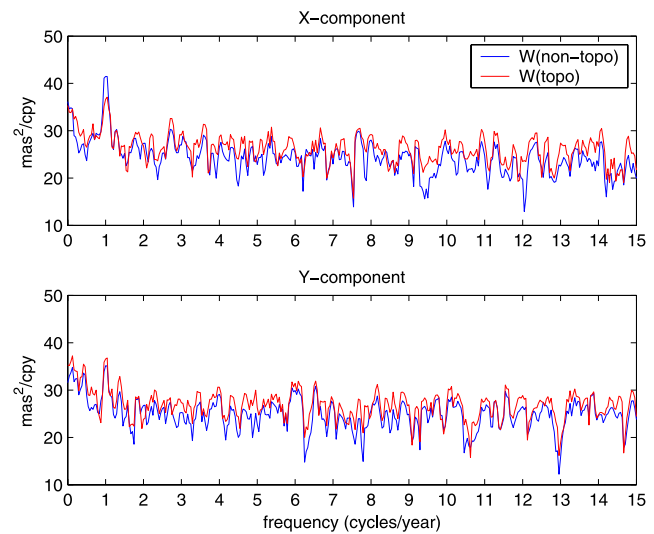


**Figure 10.** Multitaper power spectral density estimates in decibels (unit:  $\text{mas}^2/\text{cpy}$ ) of  $W(\text{nontopo})$  and  $W(\text{topo})$  for x-components (top) and y-components (bottom). A linear term is removed from each series prior to the power spectrum computation.



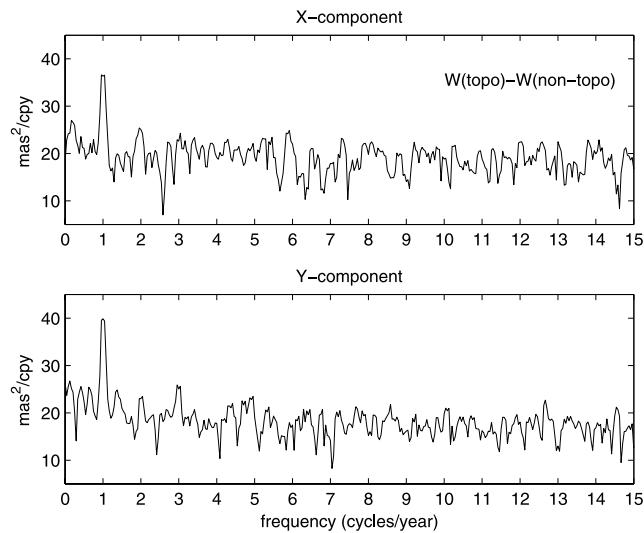


**Figure 11.** Surface topography effects on the equatorial wind AEFs in the frequency domain, shown by multitaper power spectral density estimates in decibels (unit:  $\text{mas}^2/\text{cpy}$ ) of the difference between  $W(\text{topo})$  and  $W(\text{nontopo})$  for x-components (top) and y-components (bottom).

effect is included, the correlation between the PMEF and the sum of AEF pressure and wind goes slightly higher (from 0.60 to 0.63, 0.70 to 0.71, and 0.68 to 0.69 for x, y, and  $x + iy$  components, respectively) which confirms the frequency-domain coherence analyses in section 3.2.1. Moreover, the total atmospheric effect can explain 3%, 2.4%, and 2.5% more observed x, y, and  $x + iy$  components, respectively, of

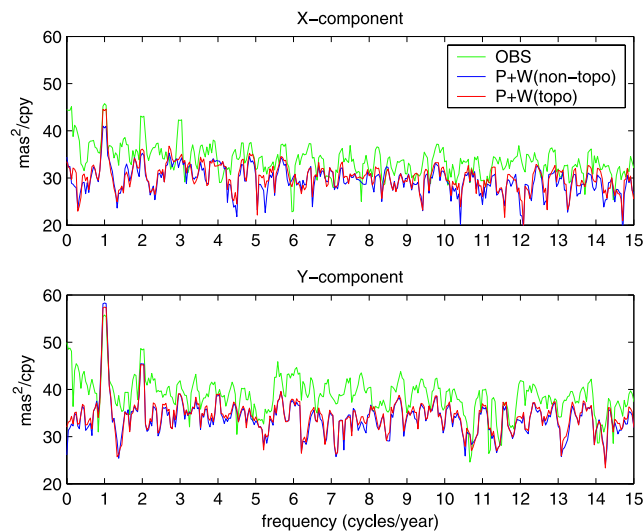


**Figure 12.** Multitaper power spectral density estimates in decibels (unit:  $\text{mas}^2/\text{cpy}$ ) of OBS (green curves),  $P+W(\text{non-topo})$  (blue curves) and  $P+W(\text{topo})$  (red curves) for x-components (top) and y-components (bottom). A linear term is removed from each series before the computation of the power spectrum. OBS: the polar motion excitation function (PMEF) inferred from SPACE2003 polar motion; P: the AEF pressure term under the inverted barometer (IB) assumption.

the intraseasonal polar motion excitation. *Gross et al. [2003]* illustrated that the global oceans, as the second important source other than the atmosphere, can explain about 20% of the intraseasonal polar motion excitation. Then, the contribution from the surface topography on the polar motion reaches equivalently over 1/10 of that of global oceans, which could be useful to closure of the Earth’s angular momentum budget in the future.

#### 4. Summary

[20] In this study, the AEF wind terms during the period of 1948–2004 are reprocessed using the NCEP/NCAR

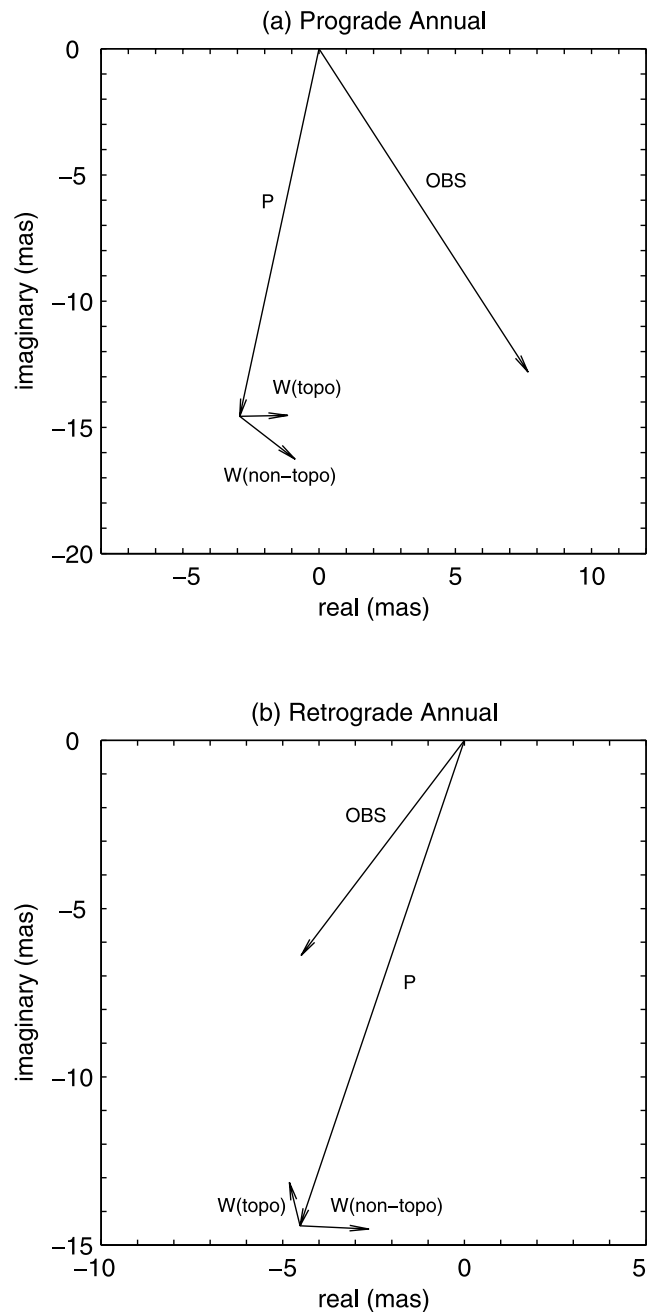


**Figure 13.** Phasor diagrams of the prograde and retrograde components of annual AEF and PMEF.

**Table 1.** Amplitude and Phase of the Prograde and Retrograde Components of the Annual Atmospheric Excitation Function (AEF) and Polar Motion Excitation Function (PMEF)<sup>a</sup>

Excitation Function	Annual Prograde		Annual Retrograde	
	Amplitude, mas	Phase, deg	Amplitude, mas	Phase, deg
OBS	14.93	-59.1	7.81	-125.1
P	14.85	-101.3	15.12	-107.4
W(nontopo)	2.64	-39.9	1.89	-2.8
W(topo)	1.75	1.1	1.32	102.9
P+W(nontopo)	16.27	-93.1	14.75	-100.3
P+W(topo)	14.57	-94.6	14.00	-110.1

<sup>a</sup>The reference date for phase is 1 January 1980, 0000 UT. OBS: the PMEF inferred from SPACE2003 polar motion; P: the AEF pressure term under the inverted barometer assumption; W(nontopo): AEF wind term without consideration of surface topography; W(topo): AEF wind term with consideration of surface topography.

reanalysis 6-hourly wind and pressure fields (products available at IERS SBA website, <http://www.aer.com/scienceResearch/diag/sb.html>). Some previous calculations with the NCEP/NCAR reanalyses are approximate in that the wind terms are integrated from an isobaric lower boundary at 1000 hPa. To consider the Earth's topography effect, however, the AEF is computed by integration using the winds from the NCEP model's representation of the Earth's surface pressure level to the top (10 hPa) analysis level. With respect to these two cases, only a minor difference, equivalent to  $\sim 0.004$  ms in LOD, exists in the axial wind term. However, considerable differences, equivalent to 5~6 milliarseconds in polar motion, are found in the equatorial wind terms. We show how Earth's topography in various layers contributes to this wind effect. We further compare the

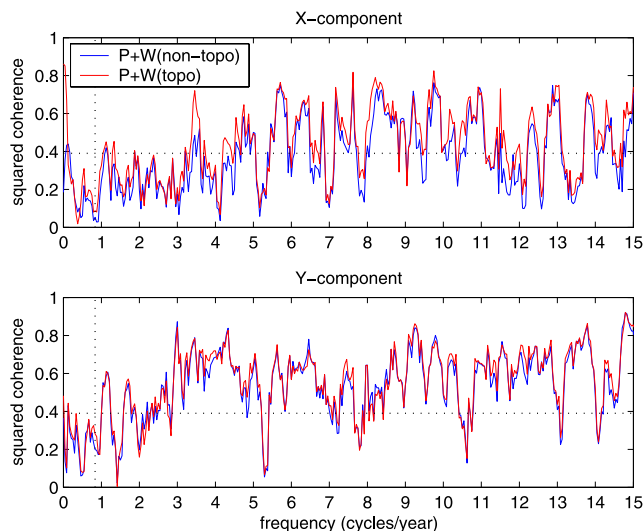


**Figure 14.** Multitaper squared coherences for x-components (top) and y-components (bottom) between the PMEF spanning 1980–2003 and the excitation functions due to P+W(nontopo) (blue curves) and P+W(topo) (red curves). A trend and a seasonal signal have been removed from each series prior to the coherence analysis. The horizontal dashed line represents the 95% significance level. The vertical dashed line indicates the Chandler frequency of 0.843 cycles per year.

**Table 2.** Cross-Correlation Coefficients Between the Intraseasonal PMEF and AEF, and Variance Reductions (in Percentage) When the Atmospheric Effects Are Removed From the PMEF<sup>a</sup>

AEF	X		Y		X + i Y	
	Corr. Coef.	Reduced Var., %	Corr. Coef.	Reduced Var., %	Corr. Coef.	Reduced Var., %
P	0.44	18.8	0.65	41.9	0.60	35.4
W(nontopo)	0.47	21.4	0.51	19.4	0.48	19.9
W(topo)	0.50	24.8	0.50	21.5	0.49	22.4
P+W(nontopo)	0.60	35.5	0.70	48.5	0.68	44.9
P+W(topo)	0.63	38.5	0.71	50.9	0.69	47.4

<sup>a</sup>X: x component; Y: y component; Corr. Coef.: Correlation coefficient; Reduced Var.: Reduced variance.

equatorial AEF, with and without the topography effect, to the polar motion excitation during the period of 1980–2003. The equatorial AEF gets generally closer to the polar motion excitation, and improved coherences are found between them when the topography effect is included.

[21] **Acknowledgments.** We are grateful to three anonymous reviewers for their insightful comments, which led to improvements in the presentation. We thank B.F. Chao and R. Ponte for their helpful discussions. Special thanks went to the Descartes-Nutation Committee, with chair, V. Dehant, Royal Observatory of Belgium, for having supported Y.H. Zhou's stay at AER for this study. Y.H. Zhou was supported in part by the National Natural Science Foundation of China (10273018, 10133010) and the Key Project of Chinese Academy of Sciences (KJ951-A1-01). D.A. Salstein was supported in part by the U.S. National Science Foundation (under grant ATM-0429975) and both he and J.L. Chen were supported by the NASA Solid Earth and Natural Hazards Program (under grants NNG04G060G, NNG04GP70G). D.A. Salstein was a visiting scientist at NASA through the University of Maryland Baltimore County GEST program during part of the study.

## References

- Aoyama, Y. (2005), Quasi-14 month wind fluctuation and excitation of the Chandler wobble, in *Proceedings of the Chandler Wobble Workshop 2004*, pp. 135–141, Eur. Cent. for Geodyn. and Seismol., Luxembourg.
- Aoyama, Y., and I. Naito (2000), Wind contribution to the Earth's angular momentum budgets in seasonal variation, *J. Geophys. Res.*, *105*, 12,417–12,431.
- Barnes, R., R. Hide, A. White, and C. R. Wilson (1983), Atmospheric angular momentum functions, length-of-day changes and polar motion, *Proc. R. Soc. London*, *387*, 31–73.
- Chao, B. F., and A. Y. Au (1991), Atmospheric excitation of the Earth's annual wobble: 1980–1988, *J. Geophys. Res.*, *96*, 6577–6582.
- Chao, B. F., and Y. H. Zhou (1999), Meteorological excitation of interannual polar motion by the North Atlantic Oscillation, *J. Geodyn.*, *27*, 61–73.
- Chao, B. F., J. B. Merriam, and Y. Tamura (1995), Geophysical analysis of zonal tidal signals in length of day, *Geophys. J. Int.*, *122*, 765–775.
- Chen, J. L., and C. R. Wilson (2005), Hydrological excitations of polar motion, 1993–2002, *Geophys. J. Int.*, *160*, 833–839.
- Chen, J. L., C. R. Wilson, X. G. Hu, Y. H. Zhou, and B. D. Tapley (2004), Oceanic effects on polar motion determined from an ocean model and satellite altimetry: 1993–2001, *J. Geophys. Res.*, *109*, B02411, doi:10.1029/2003JB002664.
- Eubanks, T. M. (1993), Variations in the orientation of the earth, in *Contributions of Space Geodesy to Geodynamic: Earth Dynamics, Geodyn. Ser.*, edited by D. Smith and D. Turcotte, pp. 1–54, AGU, Washington, D. C.
- Eubanks, T. M., J. A. Steppe, J. O. Dickey, R. D. Rosen, and D. A. Salstein (1988), Causes of rapid motions of the Earth's pole, *Nature*, *334*, 115–119.
- Gross, R. S. (2004), Combinations of Earth orientation measurements: SPACE2003, COMB2003, and POLE2003, *JPL Publ. 04-12*, Jet Propul. Lab., Pasadena, Calif.
- Gross, R. S., I. Fukumori, and D. Menemenlis (2003), Atmospheric and oceanic excitation of the Earth's wobbles during 1980–2000, *J. Geophys. Res.*, *108*(B8), 2370, doi:10.1029/2002JB002143.
- Hide, R., and J. O. Dickey (1991), Earth's variable rotation, *Science*, *253*, 629–637.

- Hide, R., J. O. Dickey, S. L. Marcus, R. D. Rosen, and D. A. Salstein (1997), Atmospheric angular momentum fluctuations during 1979–1988 simulated by global circulation models, *J. Geophys. Res.*, *102*, 16,423–16,438.
- Hsu, H. H., and B. J. Hoskins (1989), Tidal fluctuations as seen in ECMWF data, *Q. J. R. Meteorol. Soc.*, *115*, 247–264.
- Johnson, T. J., C. R. Wilson, and B. F. Chao (1999), Oceanic angular momentum variability estimated from the parallel ocean climate model, 1988–1998, *J. Geophys. Res.*, *104*, 25,183–25,195.
- Kalnay, E., et al. (1996), The NCEP/NCAR 40-year reanalysis project, *Bull. Am. Meteorol. Soc.*, *77*, 437–471.
- Masaki, Y., and Y. Aoyama (2005), Seasonal and non-seasonal AAM functions from different reanalysis data sets, in *Proceedings of the Chandler Wobble Workshop 2004*, pp. 103–108, Eur. Cent. for Geodyn. and Seismol., Luxembourg.
- Munk, W. H., and G. J. F. MacDonald (1960), *The Rotation of the Earth: A Geophysical Discussion*, Cambridge Univ. Press, New York.
- Naito, I., N. Kikuchi, and K. Yokoyama (1987), Results of estimating the atmospheric effective angular momentum functions based on the JMA global analysis data, *Publ. Int. Latitude Obs. Mizusawa*, *20*, 1–11.
- Naito, I., Y. H. Zhou, M. Sugi, R. Kawamura, and N. Sato (2000), Three-dimensional atmospheric angular momentum simulated by the Japan Meteorological Agency model for the period of 1955–1994, *J. Meteorol. Soc. Jpn.*, *78*, 111–122.
- Peixoto, J. P., and A. H. Oort (1992), *Physics of Climate*, Am. Inst. of Phys., Melville, N. Y.
- Ponte, R. M., and D. Stammer (1999), Role of ocean currents and bottom pressure variability on seasonal polar motion, *J. Geophys. Res.*, *104*, 23,393–23,410.
- Rosen, R. D., and D. A. Salstein (1985), Contribution of stratospheric winds to annual and semiannual fluctuations in atmospheric angular momentum and the length of day, *J. Geophys. Res.*, *90*, 8033–8041.
- Salstein, D. A., and R. D. Rosen (1997), Global momentum and energy signals from reanalysis systems, in *7th Conference on Climate Variations*, pp. 344–348, Am. Meteorol. Soc., Boston, Mass.
- Salstein, D. A., D. M. Kann, A. J. Miller, and R. D. Rosen (1993), The sub-bureau for atmospheric angular momentum of the interannual earth rotation service: a meteorological data center with geodetic applications, *Bull. Am. Meteorol. Soc.*, *74*, 67–80.
- Thomson, D. J. (1982), Spectrum estimation and harmonic analysis, *IEEE Proc.*, *70*, 1055–1096.
- Wiley, J. (1979), *Programs for Digital Signal Processing*, IEEE Press, Piscataway, N. J.
- Wilson, C. R. (1985), Discrete polar motion equations, *Geophys. J. R. Astron. Soc.*, *80*, 551–554.
- Wilson, C. R., and R. O. Vicente (1990), Maximum likelihood estimates of polar motion parameters, in *Variations in Earth Rotation, Geophys Monogr. Ser.*, vol. 59, edited by D. D. McCarthy and W. E. Carter, pp. 151–155, AGU, Washington, D. C.
- Zhou, Y. H., D. W. Zheng, N. H. Yu, and X. H. Liao (2001), Movement of Earth rotation and activities of atmosphere and ocean, *Chin. Sci. Bull.*, *46*, 881–888.
- Zhou, Y. H., J. L. Chen, X. H. Liao, and C. R. Wilson (2005), Oceanic excitations on polar motion: A cross comparison among models, *Geophys. J. Int.*, *162*, 390–398.

---

J. L. Chen, Center for Space Research, University of Texas at Austin, Austin, TX 78712, USA.

D. A. Salstein, Atmospheric and Environmental Research, Inc., Lexington, MA 02421, USA.

Y. H. Zhou, Shanghai Astronomical Observatory, Chinese Academy of Sciences, Shanghai 20030, China. (yhzhou@shao.ac.cn)